

# Detecting causality from time series in a machine learning framework

Cite as: Chaos **30**, 063116 (2020); <https://doi.org/10.1063/5.0007670>

Submitted: 16 March 2020 . Accepted: 19 May 2020 . Published Online: 04 June 2020

 Yu Huang,  Zuntao Fu, and  Christian L. E. Franzke



View Online



Export Citation



CrossMark

## ARTICLES YOU MAY BE INTERESTED IN

[Causal network reconstruction from time series: From theoretical assumptions to practical estimation](#)

[Chaos: An Interdisciplinary Journal of Nonlinear Science](#) **28**, 075310 (2018); <https://doi.org/10.1063/1.5025050>

[Introduction to Focus Issue: When machine learning meets complex systems: Networks, chaos, and nonlinear dynamics](#)

[Chaos: An Interdisciplinary Journal of Nonlinear Science](#) **30**, 063151 (2020); <https://doi.org/10.1063/5.0016505>

[Reconstructing directional causal networks with random forest: Causality meeting machine learning](#)

[Chaos: An Interdisciplinary Journal of Nonlinear Science](#) **29**, 093130 (2019); <https://doi.org/10.1063/1.5120778>



AIP Advances  
Mathematical Physics Collection

**READ NOW**

# Detecting causality from time series in a machine learning framework

Cite as: Chaos 30, 063116 (2020); doi: 10.1063/5.0007670

Submitted: 16 March 2020 · Accepted: 19 May 2020 ·

Published Online: 4 June 2020



View Online



Export Citation



CrossMark

Yu Huang,<sup>1</sup> Zuntao Fu,<sup>1,a)</sup> and Christian L. E. Franzke<sup>2,3</sup>

## AFFILIATIONS

<sup>1</sup>Laboratory for Climate and Ocean-Atmosphere Studies, Department of Atmospheric and Oceanic Sciences, School of Physics, Peking University, Beijing 100871, China

<sup>2</sup>Meteorological Institute, University of Hamburg, Hamburg 20144, Germany

<sup>3</sup>Center for Earth System Research and Sustainability, University of Hamburg, Hamburg 20144, Germany

<sup>a)</sup>Author to whom correspondence should be addressed: [fuzt@pku.edu.cn](mailto:fuzt@pku.edu.cn)

## ABSTRACT

Detecting causality from observational data is a challenging problem. Here, we propose a machine learning based causality approach, Reservoir Computing Causality (RCC), in order to systematically identify causal relationships between variables. We demonstrate that RCC is able to identify the causal direction, coupling delay, and causal chain relations from time series. Compared to a well-known phase space reconstruction based causality method, Extended Convergent Cross Mapping, RCC does not require the estimation of the embedding dimension and delay time. Moreover, RCC has three additional advantages: (i) robustness to noisy time series; (ii) computational efficiency; and (iii) seamless causal inference from high-dimensional data. We also illustrate the power of RCC in identifying remote causal interactions of high-dimensional systems and demonstrate its usability on a real-world example using atmospheric circulation data. Our results suggest that RCC can accurately detect causal relationships in complex systems.

© 2020 Author(s). All article content, except where otherwise noted, is licensed under a Creative Commons Attribution (CC BY) license (<http://creativecommons.org/licenses/by/4.0/>). <https://doi.org/10.1063/5.0007670>

Identifying causal relationships from observational data is crucial for understanding complex systems, and there is a need to improve causal detecting techniques. Recently, phase space reconstruction based causality methods, such as convergent cross mapping, have successfully improved our ability to detect nonlinear causality [e.g., Sugihara *et al.*, Science 338 (6106), 496–500 (2012)]. However, it is known that most algorithms of phase space reconstruction, used in causality identification, are sensitive to the presence of noise. Here, we employ a newly developed neural computing framework called Reservoir Computing to infer causality from time series. Our method can seamlessly identify causal relationships of linear and nonlinear coupled systems, including the causal direction, causal intensity, and coupling delay. Compared to convergent cross mapping, our method does not require the estimation of the embedding dimension and delay time for phase space reconstruction. Our method has the two advantages: it is robust even for noisy time series and it is computationally more efficient.

## I. INTRODUCTION

Identifying causal relationships from observational time series is a key step toward understanding complex systems such as the climate system, ecological networks, neural networks, and finance.<sup>1–6</sup> In the past few decades, various methods were developed for inferring causality,<sup>7–13</sup> such as the Granger method,<sup>1</sup> the transfer entropy method,<sup>7,13</sup> and convergent cross mapping<sup>4,10</sup> (CCM), among others. However, developing causal techniques is still a challenging issue,<sup>11–14</sup> which is partly due to the complexity of real-world systems, including nonlinearities, coupling delays, high dimensionality of the underlying dynamics, and the presence of noise in time series.

Granger<sup>1</sup> was the first to propose criteria for the detection of causal relationships: if a variable  $X$  is causing a change in variable  $Y$ , then the current values of  $X$  will be able to improve the prediction of  $Y$ 's future values with the optimal model. Takens then suggested an alternative criterion<sup>11</sup> if  $X$  causes  $Y$ , then the current values of  $Y$  can be used to reconstruct the past evolution of  $X$ . Both approaches

pay attention to a common point, that the information content of  $X$  is carried forward through time to  $Y$ ; thus, the states of  $X$  from the past share the same information with the state of  $Y$  at a later time.<sup>10</sup> In the Granger causality method, the linear regression model that relies on a linear correlation between two variables is used to test whether a variable can improve the prediction of another variable and whether this causal relationship is significant.<sup>1,9,12,13,16</sup> However, this approach has been demonstrated to perform poorly for nonlinear dynamical systems, where the variables are nonlinearly coupled and linear correlation is potentially absent or misleading.<sup>2,12,14,16</sup> In order to improve the usability to nonlinear systems, some causal methods no longer use a linear regression model but employ a phase space reconstruction technique<sup>15,17</sup> to analyze the time series, such as the causal methods of transfer entropy<sup>7,13</sup> and CCM.<sup>2,10</sup> Subsequently, the causality criteria proposed by Granger and Takens have been validated and generalized in many linear and nonlinear systems.<sup>2,4,6,7,10,12–14</sup>

In recent years, the ability of causal methods applied to various complex systems are still discussed and developed.<sup>10–14,18,19</sup> For example, it has been shown that many causal detection methods fail in the case of “generalized synchrony”<sup>20</sup> induced by a strong unidirectional forcing.<sup>2,10,18–20</sup> In this situation, Sugihara *et al.*<sup>2</sup> and Ye *et al.*<sup>10</sup> found that the dynamics of the responding variable is uniquely dominated by the driving variable, and the full system (containing both the responding and driving variables) collapses to the dynamics of the driving variable.<sup>20</sup> Although the driving variable is not caused by the responding variable, the strong forcing results in equal information content of both variables at each instantaneous moment,<sup>20</sup> and so CCM observes bidirectional causality.<sup>2,10,12,18</sup> Therefore, an extended CCM method<sup>10,19</sup> based on time-lagged statistics (we will discuss it below) was suggested to be a way to solve this issue. However, the challenges from the presence of noise and a high computational expense are still unsolved.<sup>12–14</sup>

When using causal methods based on phase space reconstruction techniques,<sup>7,12,13,21,22</sup> it is indispensable to set suitable phase space parameters, such as the embedding dimension and the time delay.<sup>17,23</sup> However, studies suggest three limitations for such pre-processing: (i) different types of algorithms for estimating phase space parameters often give inconsistent results, and so far no consensus has been reached which approach is the most reliable;<sup>22–29</sup> (ii) the estimation accuracy will easily suffer from the presence of noise, the window length, and high dimensionality of the data;<sup>10,23–30</sup> and (iii) the algorithm for selecting the phase space parameters is computationally demanding.<sup>14,22,23,27</sup> All these issues call for improved methods that can be reliably applied to real-world data.<sup>12,14,30</sup> In this study, we will contribute to addressing these issues by developing a novel causality detecting method.

In recent studies,<sup>10,11,19</sup> a newly developed CCM method (called Extended Convergent Cross Mapping, ECCM<sup>10</sup>) revealed the association between causality and cross prediction of two interacting variables: in a dynamical system with variable  $X$  causing another variable  $Y$ , with the system information propagating through time,<sup>15,24</sup> the transferred information from  $X$  to  $Y$  will be well encoded in the states of  $Y$  at later times.<sup>10,15</sup> ECCM then reconstructs the phase space attractor of  $Y$  by using the time series of  $Y$  and finds some values of  $X$  at previous times, which can be well recovered from the current

value of  $Y$  with the phase space algorithm. That is, when using  $Y$  to make lagged predictions for  $X$ , the optimal prediction will occur at a negative lag.<sup>10,11,19</sup> This result of the ECCM analysis is from the prediction model based on phase space reconstruction, and it is also consistent with Takens’s criterion.<sup>10,15</sup> However, it is still an open question whether this will be consistent when using other prediction techniques.

In this study, we exploit a newly developed machine learning prediction algorithm, Reservoir Computing<sup>31</sup> (RC), to test and generalize the conclusions of the ECCM. RC has been demonstrated to be able to skillfully reconstruct and predict time series from different nonlinear dynamical systems.<sup>32–38</sup> Compared with other neural computing frameworks that are applicable to sequential data (time series), such as Long Short-Term Memory network and Artificial Neural Network based on Backpropagation,<sup>37–39</sup> RC has been demonstrated to be superior<sup>35,38</sup> with respect to simulating the probability density function, variance, and prediction skill. Specifically, the neuron state of RC can track the temporal evolution of time series,<sup>32–38</sup> but the neurons of Artificial Neural Networks based on Backpropagation cannot.<sup>37–39</sup> The ability to track temporal evolution for neuron states is crucial for accurately simulating dynamical time series.<sup>37–39</sup> More importantly, current research<sup>35</sup> reveals that RC can also reconstruct the attractors of nonlinear dynamical systems, where the Poincaré return map and Lyapunov exponent of the attractor were well recovered by RC, but does not require the pre-selection of phase space parameters.<sup>32–38</sup> Accordingly, when using RC to reconstruct the attractor and then to estimate the causal relationship as ECCM does, the above-mentioned issues induced by the phase space parameters will be improved. We name this new approach the RC-based causality method (RCC), and in this article, its ability will be systematically compared with ECCM.

There are three characteristics that are crucial to identify causal relationships: the direction of the causal relationship ( $X$  causes  $Y$  or  $Y$  causes  $X$ ),<sup>1–6</sup> the intensity of causal interactions,<sup>2,10,13,19,38</sup> and the delay between cause and effect (coupling delay).<sup>10,11,19</sup> For investigating the ability of RCC to identify these causal relationships, we will analyze these three characteristics of causal relationships in bivariate systems that have been previously used for causality studies.<sup>2,7–13</sup> We will pay attention to the improvements of the computational cost and the robustness to the presence of noise when using RCC. Finally, based on the ability to identify coupling delays, we will also present a potential application of RCC in the remote causal interactions of high-dimensional systems. Through these systematic investigations on RCC, we demonstrate its usefulness for real-world problems.

In Secs. II–VI of this article, we will first show the algorithms of the RC and phase space prediction models, which will be used by the RCC and ECCM methods, respectively. Then, we will present how the RCC method works for the causal inference, and the relation between RCC and ECCM. Also, we will demonstrate the ability of RCC to identify causal relationships by applying it to model simulated time series. Subsequently, we demonstrate the superiority of our method compared with ECCM and present examples of its application to transitive causal chain and atmospheric circulation data.

## II. METHOD

### A. Reservoir computing prediction model

Assuming that  $X$  and  $Y$  are two variables from an arbitrary system, hereafter we use  $X(t)$  and  $Y(t)$  to denote the observed time series of  $X$  and  $Y$  ( $t$  is a set of integer numbers to present the time order in a time series). The Reservoir Computing prediction model<sup>31–38</sup> can estimate the value of  $Y(t + \tau)$  from  $X(t)$ , where  $\tau$  denotes the time lag and “ $\tau = 0$ ” indicates the instantaneous estimation of  $Y(t)$  from  $X(t)$ ; “ $\tau < 0$ ” means that we use  $X(t)$  to reconstruct the values of  $Y$  at previous times; “ $\tau > 0$ ” means that we use  $X(t)$  to estimate future values of  $Y$ . Here, the used RC neural computing framework includes three layers (Fig. 1): the input-to-reservoir layer, the reservoir neuron layer, and the reservoir-to-output layer. Hence, in order to estimate  $Y(t + \tau)$  from  $X(t)$ , the RC prediction model carries out the following steps:

- (i)  $X(t)$  (a vector with dimension  $L$ ) first goes through the input-to-reservoir layer to the reservoir neuron layer. There are four components: the initial reservoir neuron state  $r(t)$  (a vector of dimension  $N$ , representing the activation of the  $N$  neurons of this neural network), the adjacent matrix  $M$  (of size  $N \times N$ ) representing connectivity of the  $N$  neurons, the input-to-reservoir weight matrix  $W_{in}$  (of size  $N \times L$ ), and an unit matrix  $E$  (of size  $N \times N$ ,  $E$  is used to reduce the bias in the training<sup>34</sup>). The association between the components is given by

$$r^*(t) = \tanh [M \cdot r(t) + W_{in} \cdot X(t) + E], \quad (1)$$

where  $r^*(t)$  denotes the updated neuron state. Equation (1) shows a variant of the reservoir state updating equations,<sup>31</sup> and this variant has been demonstrated to be able to well simulate the temporal dynamics of linear and nonlinear systems.<sup>32,34,35,38</sup> Other variants of the reservoir state updating equations will be further investigated in the future.

- (ii)  $r^*(t)$  then gets into the third layer consisting of the reservoir-to-output matrix  $W_{out}$

$$\hat{Y}(t + \tau) = W_{out} \cdot r^*(t). \quad (2)$$

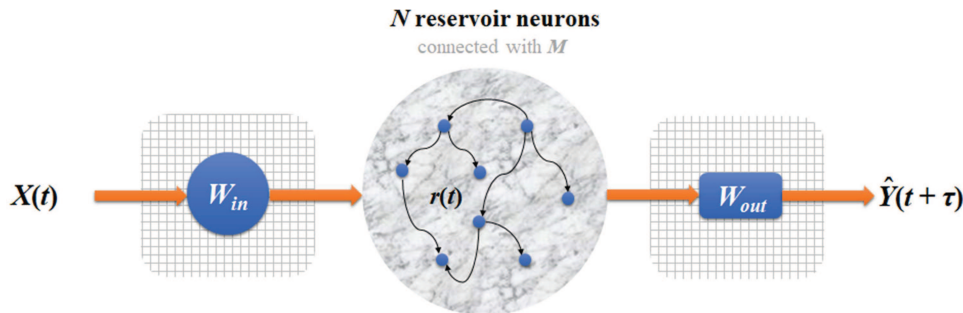


**FIG. 1.** A schematic of Reservoir Computing prediction.  $X(t)$  is the input for the training. The input-to-reservoir layer consists of a matrix  $W_{in}$  (whose elements are randomly chosen from the interval  $[-1, 1]$ ). The neuron layer consists of  $N$  reservoir neurons whose connectivity is through the Erdős–Renyi complex network<sup>39</sup>  $M$ , and  $r(t)$  represents the activations of the  $N$  neurons. The reservoir-to-out layer consists of a matrix  $W_{out}$ , which is used to fit the relation between neuron activations and  $Y(t + \tau)$ .  $W_{in}$  and  $M$  are preset at the beginning of training and fixed during training and testing. Only  $W_{out}$  is trainable during training. After the RC is trained, it can be used for prediction and  $\hat{Y}(t + \tau)$  denotes the predicted time series.

As Eq. (2) shows,  $r^*(t)$  will be used to estimate  $Y(t + \tau)$ , where the estimated value is denoted as  $\hat{Y}(t + \tau)$ .  $W_{out}$  is the trainable matrix that captures the relation between  $r^*(t)$  and  $Y(t + \tau)$  during the training process, and its mathematical form is given by

$$W_{out} = \arg \min_{W_{out}} ||W_{out} \cdot r^*(t) - Y(t + \tau)|| + \alpha ||W_{out}||, \quad (3)$$

The symbol  $|||$  represents the  $L_2$ -norm of a vector and  $\alpha$  is the ridge regression coefficient (the least square method is used), whose values will be determined after the training period.

- (III) After performing these reservoir operations, the neural network is trained, and we can use it to predict  $Y(t + \tau)$ , where the predicted series is denoted as  $\hat{Y}(t + \tau)$ . In our study, the time series was divided into training (40%) and testing (60%) sets, and then both sets will be further used to evaluate the prediction skill (see Sec. III about causal inference).

The settings for the components in Eq. (1) are as follows: (i) The adjacent matrix  $M$  determines the connectivity structure of this reservoir neural network, and this constitutes a sparse Erdős–Renyi complex network configuration,<sup>34,40</sup> whose elements are randomly chosen from a uniform distribution in  $[-1, 1]$ . We then multiply all the elements of  $M$  by a positive scalar so that the largest eigenvalue of  $M$  becomes  $\rho$ , which is called the “spectral radius” of  $M$ .<sup>34</sup> In this study, we set the spectral radius as 1, and the average degree of this Erdős–Renyi network is set as 20. (ii) The elements of  $W_{in}$  are randomly chosen from a uniform distribution in  $[-1, 1]$ . (iii) For all analyzed time series in this paper, their data lengths ( $L$ ) are uniformly set as 10 000. Hence, we set  $N$  to 400 by considering that the optimal setting for  $N$  depends on the vector length of  $X(t)$ .<sup>31–38</sup> Here, the parameter selection refers to previous studies,<sup>32,34,38</sup> which yielded good performances. We also tested different values for the parameters and found that different values did not influence the ability of the RCC to infer the direction of causal relationships (as discussed later).  $W_{in}$  and  $M$  are set at the beginning of the training period and held fixed during training and testing. Only  $W_{out}$  is estimated during the training period.

## B. Phase space prediction model

Similarly, assuming that  $X(t)$  and  $Y(t)$  are two time series from an arbitrary system, we can also use the phase space prediction model<sup>21</sup> to estimate the value of  $Y(t + \tau)$  from  $X(t)$ . There are three steps to realize the phase space prediction from  $X(t)$  to  $Y(t + \tau)$ :

- (i) Estimating the embedding dimension ( $m$ ) and time delay ( $\tau_0$ ) for  $X$ , which we do by applying the false nearest neighbor algorithm;<sup>27</sup>
- (ii) switching  $X(t)$  to the phase space (a lagged coordinate):<sup>17,21</sup>  $X_t^{m,\tau_0} = \{x_t, x_{t-\tau_0}, \dots, x_{t-(m-1)\tau_0}\}$  is acting as the prediction vector  $M_X(t)$ ;
- (iii) predicting the value of  $Y(t + \tau)$  by

$$\hat{Y}(t + \tau) = \sum_{i=1}^{m+1} w_i Y(t_i). \quad (4)$$

The weight parameter  $w_i$  is estimated from the vectors  $M_X(t)$  and  $M_X(t_i)$ , defined as

$$w_i = \frac{u_i}{\sum_{i=1}^{m+1} u_i}, \quad (5)$$

$$u_i = \exp \left\{ -\frac{d [M_X(t), M_X(t_i)]}{d [M_X(t), M_X(t_1)]} \right\}, \quad (6)$$

where  $d [M_X(t), M_X(t_i)]$  denotes the Euclidean distance between the vectors  $M_X(t)$  and  $M_X(t_i)$ . “ $t$ ” denotes the current time and “ $t_i$ ” represents another time point (except “ $t$ ”) of the observation period. When using the phase space prediction model, the length for every analyzed time series is set as 10 000.

## C. Significance test

To check the statistical significance of our computational results, we use Monte Carlo experiments: we employ the iterative amplitude adjusted Fourier transform (IAAFT)<sup>41,42</sup> method to generate surrogate time series. IAAFT preserves the probability distribution and the autocorrelation of the original time series. For every dataset used in this paper, we generate 100 surrogate series to repeat the computation of causality and then we obtain the 95% confidence interval of the IAAFT surrogates. If the computational results of the original series exceed this confidence interval, we will claim that the calculated causal relationship is statistically significant.

## III. CAUSAL INFERENCE

To test RCC, we use a system where variable  $a$  causes a change in variable  $b$ :

$$\begin{aligned} a(t+1) &= 0.85a(t) + \varepsilon_1(t), \\ b(t+1) &= 0.80b(t) + \varepsilon_2(t) + 0.20a(t), \end{aligned} \quad (7)$$

where  $\varepsilon_1(t)$  and  $\varepsilon_2(t)$  denote Gaussian-distributed white noises with zero mean and unit variance. We now illustrate how the causal method of ECCM<sup>10</sup> works. As Fig. 2(a) shows, first  $a(t)$  is input into the phase space prediction model to estimate  $b(t + \tau)$ , and the output series is denoted as  $\hat{b}(t + \tau)$  (this is a time-lagged prediction and  $\tau$  ranges from  $-30$  to  $30$ ). Then, to evaluate the prediction skill that  $a(t)$  predicts  $b(t + \tau)$ , we adopt the Pearson correlation between

$b(t + \tau)$  (the real time series) and  $\hat{b}(t + \tau)$  (the output series from the prediction model), defined as<sup>2,5,6,10–12,19</sup>

$$\rho_{ab}(\tau) = \text{corr. } [b(t + \tau), \hat{b}(t + \tau)]. \quad (8)$$

Moreover, we also use  $b(t)$  to predict  $a(t + \tau)$  through the phase space prediction model and then measure the prediction skill with  $\rho_{ba}(\tau) = \text{corr. } [a(t + \tau), \hat{a}(t + \tau)]$ , where  $\hat{a}(t + \tau)$  is the output series from the prediction model. As Ye *et al.*<sup>10</sup> demonstrate, the causality can be inferred at different time lags ( $\tau$ ) where  $\rho_{ab}(\tau)$  and  $\rho_{ba}(\tau)$  reach their peak values:

- (i) If  $a$  uni-directionally causes  $b$ , then the current information of  $a$  is encoded in the future  $b$ <sup>24</sup> and the peak value of  $\rho_{ab}(\tau)$  will be at a positive  $\tau$ . In contrast, if the current information of  $b$  is partially from the states of  $a$  at the previous time points,<sup>15</sup> then the peak value of  $\rho_{ba}(\tau)$  will be at a negative  $\tau$ .
- (ii) If both  $a$  and  $b$  cause each other, the peak values of  $\rho_{ab}(\tau)$  and  $\rho_{ba}(\tau)$  will occur at negative lags for both.
- (iii) If the coupling of  $a$  and  $b$  has a delay effect, the lag positions of the peaks of  $\rho_{ab}(\tau)$  and  $\rho_{ba}(\tau)$  will be influenced by the delay time.

In the above steps of the ECCM, the used prediction technique to realize the cross prediction between variables is the phase space prediction model. As mentioned in the Introduction, in order to make progress, we propose to replace “the phase space prediction model” with “the RC prediction model” (RCC), and we test whether RCC can also identify causal relations.

Figure 2(b) shows the values of  $\rho_{ab}(\tau)$  at different time lags of RCC applied to the time series of Eq. (7). The peak value of  $\rho_{ab}$  occurs at lag = 2, and  $\rho_{ab}(\tau)$  obtains higher values at positive lags than at negative lags. This means that the value of  $b(t + 2)$  can be well estimated from  $a(t)$ . As the time lag ( $\tau$ ) gets much larger than 2, the value of  $\rho_{ab}(\tau)$  is getting smaller and finally is no longer statistically significant. This result is consistent with the fact that  $a$  does influence  $b$  in Eq. (7), and the future state of  $b$  is encoded in the information of  $a$ , so that the current value of  $a$  has the ability to estimate the future values of  $b$ . Similarly, Fig. 2(c) shows that  $\rho_{ba}$  obtains its maximum at lag =  $-4$ , and the value of  $a(t - 4)$  can be well recovered from  $b(t)$ .

Furthermore, we also employ ECCM to estimate the values of  $\rho_{ab}(\tau)$  and  $\rho_{ba}(\tau)$ .<sup>8,10,19</sup> Here, we use  $m = 8$  and  $\tau_0 = 1$  as the phase space parameters. Figures 2(b) and 2(c) show that, in this linear stochastic coupled system [Eq. (7)], the prediction skill peaks of RCC and ECCM are very close to each other, which suggest no difference in the ability of the phase space prediction model and RC prediction model for this linear system.

## IV. CAUSAL DETECTION IN CONCEPTUAL NONLINEAR SYSTEMS

### A. Detecting direction and intensity of causality

It is known that causal detection in nonlinear systems is more demanding than in linear systems.<sup>2,10,12,16</sup> Thus, we now investigate a conceptual bivariate nonlinear system with unidirectional coupling,

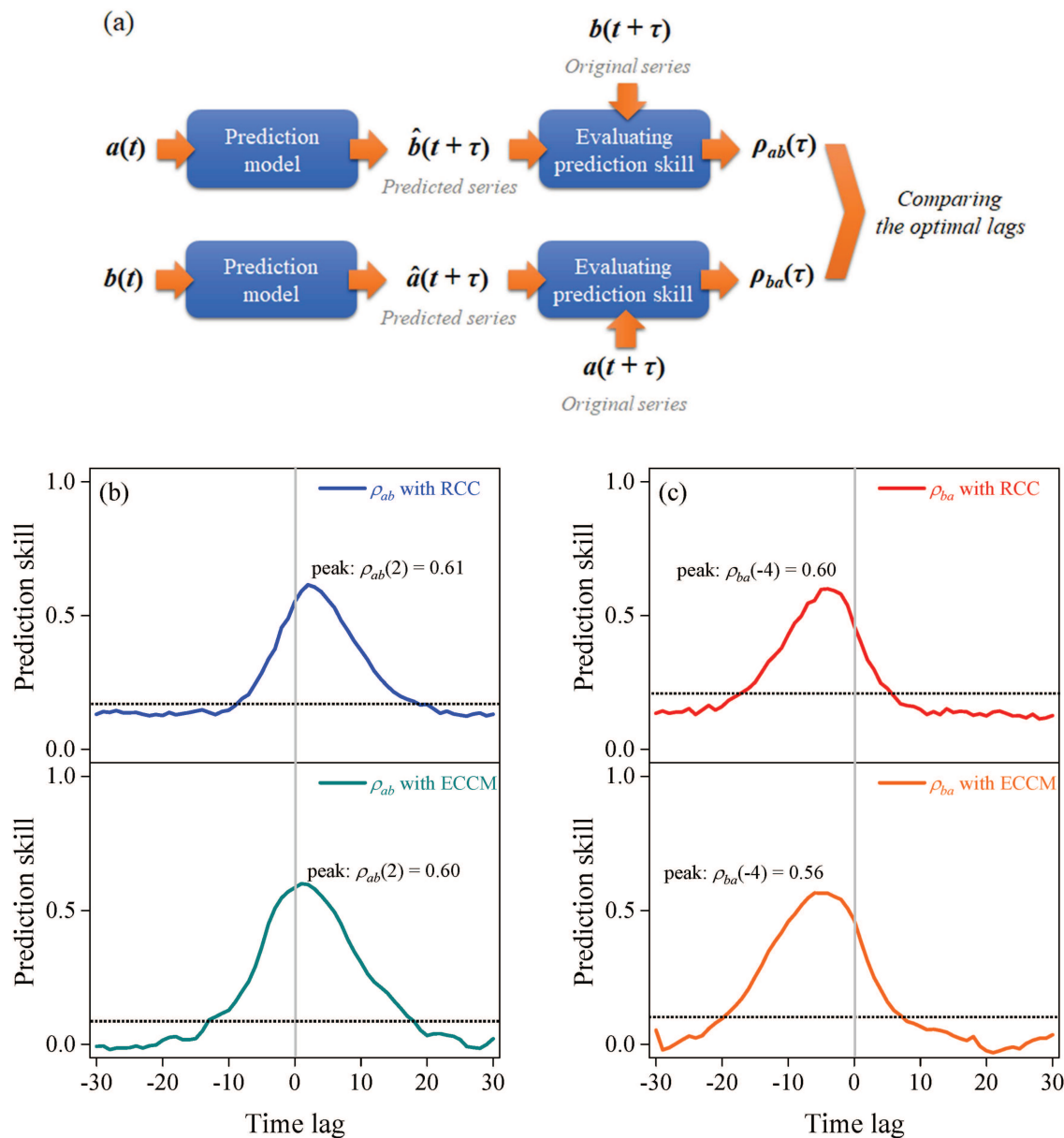


**FIG. 2.** (a) Workflow of the causal inference for both RCC and ECCM. (b) Time-lagged prediction skill that  $a(t)$  predicts “ $b$ ” (“ $t$ ” + “ $\tau$ ”). (c) Time-lagged prediction skill that  $b(t)$  predicts “ $a$ ” (“ $t$ ” + “ $\tau$ ”). The horizontal dotted lines represent the upper 95% confidence level of IAAFT surrogate test.

which is given by

$$\begin{aligned} x(t+1) &= x(t)[3.78 - 3.78x(t)], \\ y(t+1) &= y(t)[3.77 - 3.77y(t) - Cx(t)], \end{aligned} \quad (9)$$

where “ $C$ ” controls the coupling strength.

The results of RCC and ECCM applied to Eq. (9) are presented with a moderate unidirectional coupling ( $C = 0.8$ ) in Fig. 3(a) and a weak unidirectional coupling ( $C = 0.08$ ) in Fig. 3(b). For the RCC results, the peak value of  $\rho_{xy}$  occurs at lag = 6, and  $\rho_{yx}$  obtains the

maximum at lag = −1 for a moderate coupling strength [Fig. 3(a)]. All peak values in Fig. 3(a) are statistically significant. This suggests that information about  $x(t)$  is encoded in  $y(t+6)$ , and the information of  $x(t-1)$  is encoded in  $y(t)$ . The RCC method can infer the true causality that  $x$  influences  $y$ . Furthermore, it can be seen that the peak value of  $\rho_{xy}$  for weak coupling is decreased greatly due to the weakened causal coupling, but this maximum still occurs at a positive lag [Fig. 3(b)]. The weakened causal forcing does not influence the performance of the RCC technique on detecting the

true causality direction. Moreover, when the coupling strength is weakened, the value of  $\rho_{yx}$  is also decreased. This means, that the magnitude of the optimal prediction skill is affected by the causal interaction intensity.<sup>2,10,13,19,38</sup>

In Fig. 3(a), the results of RCC and ECCM show that the maximum of  $\rho_{yx}$  occurs at lag = -1, and the peak values of RCC and ECCM are the same. The peak positions of  $\rho_{xy}$  occur at positive lags for both RCC and ECCM, but positions and values of the maximal  $\rho_{xy}$  are different. The causal direction inference of RCC is identical to that of ECCM. Analyzing this system, we use  $m = 2$  and  $\tau_0 = 1$  as the phase space parameters.

Now, we investigate bidirectional causality. A bivariate nonlinear dynamical system with bidirectional coupling is given by

$$\begin{aligned} x(t+1) &= x(t)[3.78 - 3.78x(t) - 0.01z(t)], \\ z(t+1) &= z(t)[3.77 - 3.77z(t) - 0.01x(t)]. \end{aligned} \quad (10)$$

For this case, the maxima of  $\rho_{xz}$  and  $\rho_{zx}$  both occur at lag = -1 [Fig. 3(c)]. This validates the rule for bidirectional causality:<sup>10,19</sup> if  $x$  causes  $z$  ( $z$  also causes  $x$ ), the optimal prediction lags for  $\rho_{xz}$  and  $\rho_{zx}$  will be both negative. The ECCM method shows similar results as the RCC method in detecting the causality direction (see also Ye *et al.*<sup>10</sup>). We analyze this system using the phase space parameters:  $m = 2$  and  $\tau_0 = 1$ .

## B. Detecting coupling delay of causality

The cause and effect might not always occur instantaneously,<sup>10,11,19</sup> and after identifying the causal direction between two variables, it is also useful to identify whether there exists a delay between cause and effect. Hence, we will investigate

whether the methods can infer the coupling delay of causal relationships. To investigate the observational time series with known delay coupling, a bivariate nonlinear dynamical system with time-delayed coupling is given by

$$\begin{aligned} x(t+1) &= x(t)[3.78 - 3.78x(t)], \\ y(t+1) &= y(t)[3.77 - 3.77y(t) - 0.8x(t - \tau_d)]. \end{aligned} \quad (11)$$

In this experiment, the dynamic delay  $\tau_d$  ranges from 0 to 9. “ $\tau_d + 1$ ” denotes how much time the causal influence from  $x$  to  $y$  is delayed ( $\tau_d$  will range from 1 to 10 here). For every value of  $\tau_d$ , the output time series are analyzed by RCC and ECCM. Here, we also use  $m = 2$  and  $\tau_0 = 1$  as the phase space parameters of ECCM.

Figure 4 shows the results of RCC and ECCM applied to the observational time series of Eq. (11). When “ $\tau_d + 1$ ” is increased from 1 to 10, RCC and ECCM equally give the peak positions of  $\rho_{yx}$  ranging from -1 to -10 [Figs. 4(a) and 4(c)], which is consistent with the true dynamical setting of Eq. (11). However, RCC and ECCM give different results for  $\rho_{xy}$ : when “ $\tau_d + 1$ ” is increased from 1 to 10; for RCC, the corresponding peak positions of  $\rho_{xy}$  range from 6 to 14 [Fig. 4(b)], but from 12 to 22 for ECCM [Fig. 4(d)]. When we only use the peak positions of  $\rho_{xy}$ , RCC and ECCM both heavily overestimate the delay time. However, ECCM performs worse. This suggests that the estimation is more reliable for a coupling delay at negative lags. Ye *et al.*<sup>10</sup> also found that the optimal ECCM prediction skill occurring at negative lags can exactly measure the coupling delay, which is consistent with our results of RCC. However, the positive optimal lags tend to overestimate the real coupling delay, and the reason needs to be addressed in a future study since it is beyond the scope of the present study.

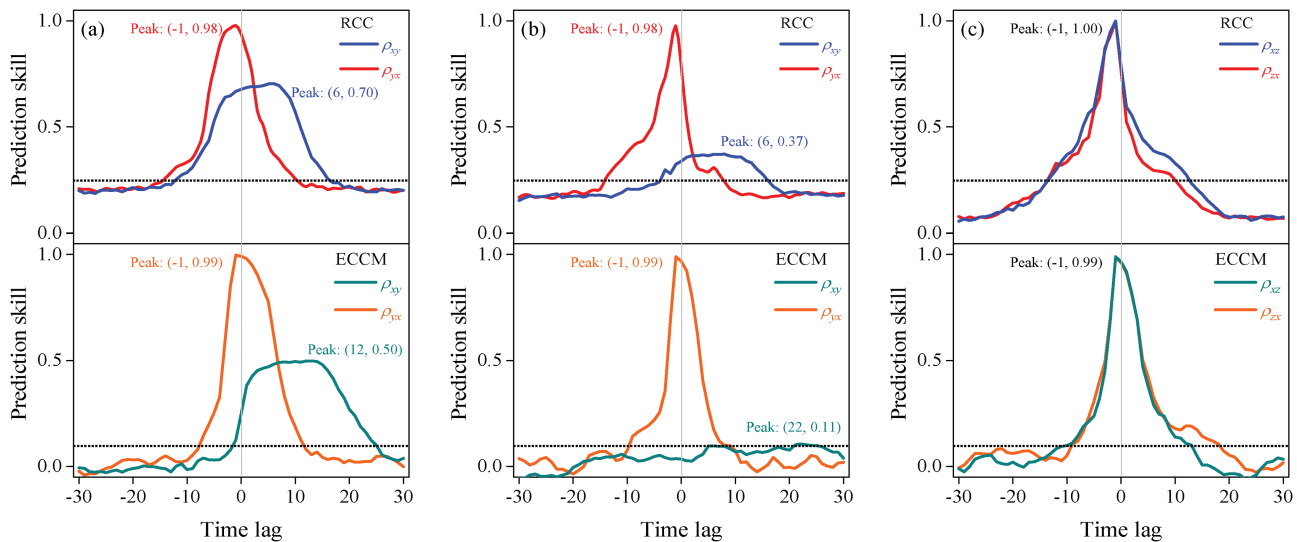


**FIG. 3.** Time-lagged prediction skill in bivariate systems with different coupling dynamics. (a) Nonlinear dynamical system with moderate unidirectional coupling [ $C = 0.8$  in Eq. (9)]. Here,  $\rho_{xy}$  denotes using  $x$  to predict  $y$ , and  $\rho_{yx}$  denotes using  $y$  to predict  $x$ . (b) Nonlinear dynamical system with weak unidirectional coupling [ $C = 0.08$  in Eq. (9)]. (c) Nonlinear dynamical system with bidirectional coupling [Eq. (10)]. The horizontal dotted lines represent the upper 95% confidence level of IAAFT surrogate test.

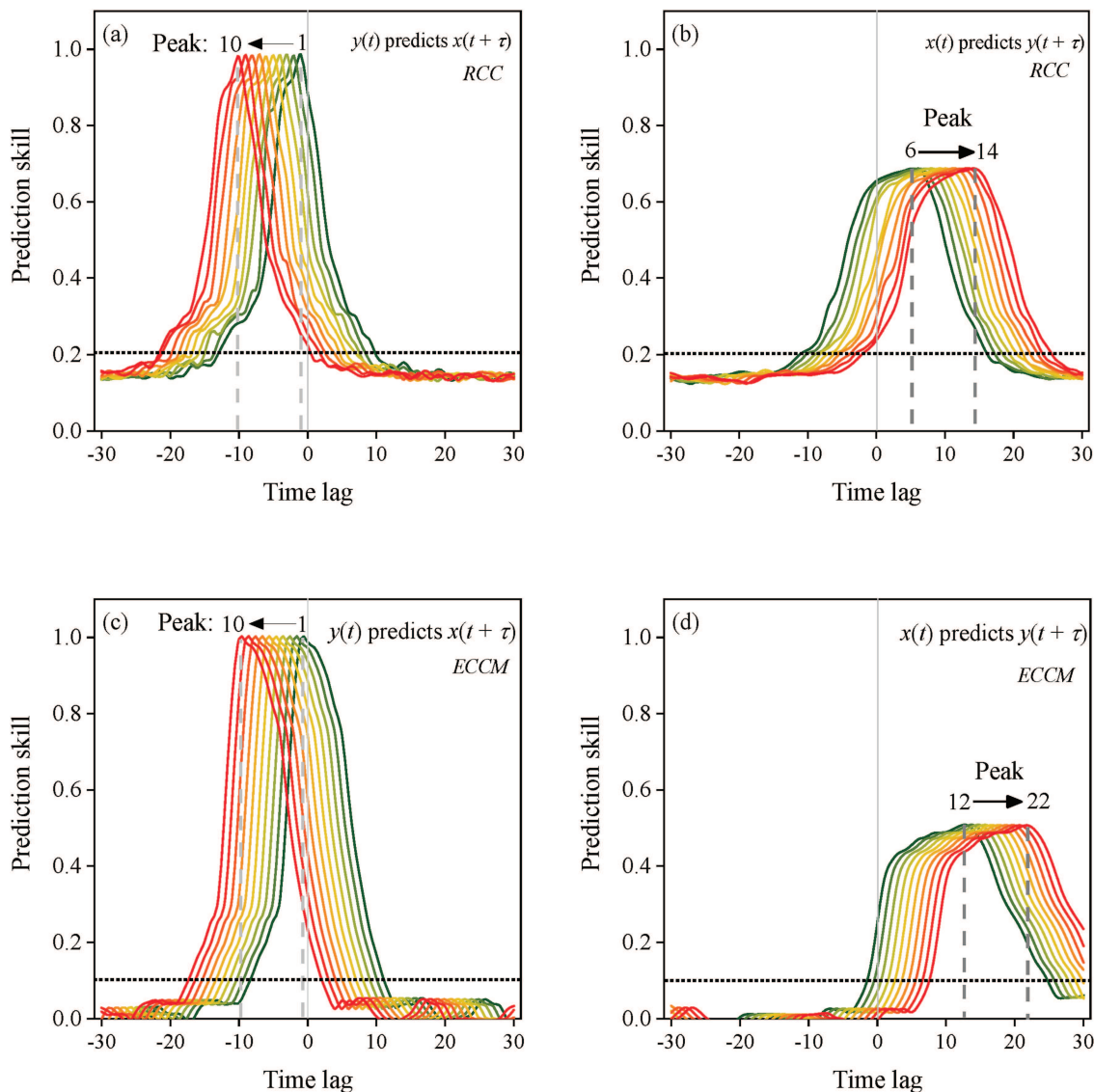


**FIG. 4.** Time-lagged prediction skill of coupled logistic systems with delayed couplings [Eq. (11)]. Using  $y(t)$  to predict  $x(t+\tau)$  by RCC (a) and ECCM (c); Using  $x(t)$  to predict  $y(t+\tau)$  by RCC (b) and ECCM (d). Delayed time ( $\tau_d + 1$ ) of the coupling is set from 1 to 10 corresponding to the colored lines from green to red. The horizontal axis denotes the used time lag for the prediction. The horizontal dotted lines represent the upper 95% confidence level of IAAFT surrogate test.

RCC and ECCM can give identical inferences for the causal direction and coupling delay, but there exists a difference in the prediction skills derived from RCC and ECCM, respectively. This may be due to the different computational algorithms of the phase space prediction model and RC. The phase space prediction model estimates values according to the local distance weighted in a lagged coordinate;<sup>21</sup> however, the RC estimates values according to a global connected complex network configuration.<sup>34,35</sup> Whether such a difference in the algorithms induces also other differences in the performances of RCC and ECCM will be addressed next.

## V. PERFORMANCE OF RCC

It is known that the presence of measurement noise and the computational expense are potential issues when dealing with real-world problems, and causal detection methods need to address these two issues.<sup>12,14,30</sup> Previous studies<sup>10,30</sup> revealed that both CCM and ECCM suffer from the influence of noisy data. There are two reasons for this: (i) as mentioned in the Introduction, before using the phase space prediction model, pre-selection of the phase space parameters cannot be very accurate, which is partially due to the high sensitivity to the presence of noise;<sup>10,23–30</sup> (ii) for the algorithm

of the phase space prediction model, it is necessary to measure the distance between two arbitrary points in the phase space, but the presence of noise tends to disturb this distance in phase space,<sup>10,24,30</sup> and the inaccuracy of the phase space parameters also introduce a bias into the phase space coordinates. Moreover, it is known that the algorithms for preselecting the phase space parameters are often computationally expensive, and the algorithm of the phase space prediction model might also demand a high amount of computational resources. We now investigate whether RCC performs better than ECCM regarding noise sensitivity and computational efficiency.

### A. Performance in the presence of noise

To test the impact from measurement noise, we standardize the time series of Eq. (9) ( $C = 0.8$ ) to zero mean and unit variance, and then mix it with Gaussian-distributed white noise with zero mean. The variance contribution of the white noise is  $R_{\text{noise}}$  (which is equal to the variance ratio of the noise to the composited time series). Figure 5(a) shows the attractors of Eq. (9) when  $R_{\text{noise}}$  is set to 0%, 4%, and 40% of the total variance, respectively. Low noise ( $R_{\text{noise}} = 4\%$ ) will slightly blur, while high noise ( $R_{\text{noise}} = 40\%$ ) will significantly blur the attractor. Since CCM and ECCM are based on reconstructing the attractor, a large impact of the noise on their performance is visible.

Figure 5 shows how the noise impacts the time-lagged prediction skill curves. For RCC, there is no impact on its performance in detecting the causality direction and coupling delay [Fig. 5(b)] when the noise is low ( $R_{\text{noise}} = 4\%$ ); even under high noise ( $R_{\text{noise}} = 40\%$ ), the performance is only slightly affected [Fig. 5(c)]. However, ECCM is already not able to estimate the correct causality direction at negative lags [Fig. 5(d)] when  $R_{\text{noise}}$  is only 4%, the uncertainty of the prediction skill increases further [Fig. 5(e)] with increasing noise amplitude ( $R_{\text{noise}} = 40\%$ ). To quantify the noise impact, we define the relative deviation as

$$\text{Relative deviation} = \sqrt{\frac{\sum_{\tau} [\rho'(\tau) - \rho(\tau)]^2}{\sum_{\tau} \rho(\tau)^2}}, \quad (12)$$

where  $\rho(\tau)$  is the time-lagged prediction skill curve free from noise and  $\rho'(\tau)$  is the distorted time-lagged prediction skill curve impacted by the noise. A larger relative deviation denotes worse robustness to the noise.

Figure 6 shows the comparison of robustness to the noise between RCC and ECCM. Our results indicate that RCC is more robust to noise with smaller uncertainty than ECCM [Fig. 6(a)], and the relative deviation of ECCM for low noise ( $R_{\text{noise}} = 4\%$ ) is comparative with those of RCC for high noise ( $R_{\text{noise}} = 40\%$ ). In addition, Fig. 6(b) shows how the peak positions vary with  $R_{\text{noise}}$ . For ECCM, the peak position of  $\rho_{yx}$  repeatedly changes between negative and positive lags, which will lead to a wrong estimation of the causality directions. For RCC, this does not happen and it always provides the true causality direction in our experiments. Thus, this test suggests that the causal inference from RCC is more reliable than ECCM.

The complex network configuration, which is used for the connectivity of the RC neural network,<sup>34,35</sup> might be responsible for the

lesser sensitivity to noise. Some recent studies<sup>43–46</sup> found that a complex network configuration can be robust to noise and that many real-world data with noise can be well analyzed. Moreover, previous studies<sup>34,35,37</sup> also showed that components of RC [like the unit matrix  $E$  in Eq. (1) and the matrix in  $W_{\text{out}}$  Eq. (3)] are useful in reducing the influence of noise and bias.

### B. Computational efficiency

Table I presents a comparison of the computational time for RCC and ECCM. It can be seen that estimating phase space parameters takes most of the computational time when inferring causality through ECCM, whereas the RCC takes much less computational time to accomplish the same task of causal inference.

### C. Effect of RC parameters

We demonstrated the ability of RCC to identify causal relationships, but it is also important to examine how RC parameters settings influence the identification of the direction and coupling delay of causal relationships. Hence, we experimented for different numbers of reservoir neurons ( $N$ ) and different reservoir network parameters (here we selected the spectral radius).

We find that choosing a different  $N$  or a different spectral radius of the reservoir network does not influence the direction inference of the causal relationships. For all analyzed systems, the peak position of the RCC curve is always at a positive lag (or a negative lag) even with different  $N$  or different spectral radius (i.e., Fig. 7), which has been determined by the relation between predictability and causal information flow<sup>10,11,13</sup> (see also Granger's and Takens's criteria<sup>1,15</sup>). This means that the driving and responding variables can always be distinguished and further demonstrate the robustness of RCC.

When  $N$  or the spectral radius of reservoir network is changed, we also find that the shape of the RCC curve is varied, and sometimes the RCC curve will even have a plateau rather than a distinguishable peak [i.e., Fig. 7(a)]. In this case, though the causal direction can still be inferred, the peak position and coupling delay cannot be identified accurately. By changing  $N$  or the spectral radius, it can be seen that the peak of the RCC curve can be sharp and highly distinguishable, and its peak position is actually fixed under different  $N$  or spectral radius [see Figs. 7(a) and 7(c)]. It was previously reported that the length of the used time series could influence the estimation of a suitable  $N$  for obtaining a good performance of RC.<sup>34–37</sup> The spectral radius of the complex network determines the features of network connectivity,<sup>34,40,46</sup> and its role in reservoir computing needs to be further addressed in future studies. Therefore, for obtaining the distinguishable coupling delay of causal relationships, the setting of reservoir neural network parameters (such as  $N$  and spectral radius) should refer to a distinguishable peak position in the RCC curve and the length of analyzed time series. In the following applications of RCC, we still use  $N = 400$  and spectral radius = 1, which yield the distinguishable peak positions for the RCC curves, and the robustness of the inferred peak positions has been inspected (not shown).

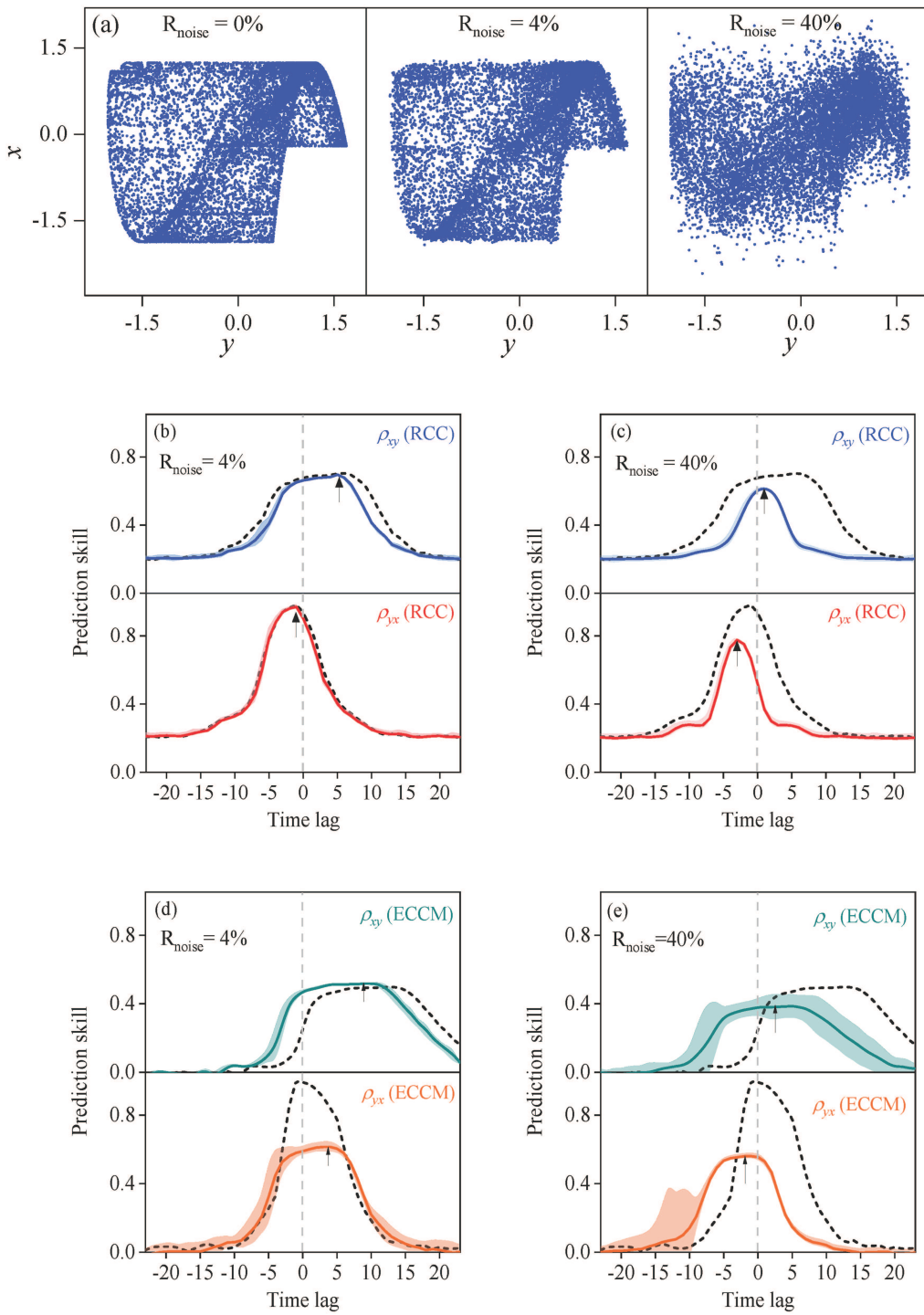


**FIG. 5.** (a) The blurred attractor of Eq. (9) ( $C = 0.8$ ) with different noise ratios. (b)  $R_{\text{noise}} = 4\%$ : prediction skill curves of RCC deviate slightly from the case of no noise (dashed lines). (c)  $R_{\text{noise}} = 40\%$ : prediction skill curves of RCC have the same phase positions as in the case of no noise (dashed lines). (d)  $R_{\text{noise}} = 4\%$ : prediction skill curves of ECCM deviate from the case of no noise (dashed lines). (e)  $R_{\text{noise}} = 40\%$ : prediction skill curves of ECCM deviate from the case of no noise (dashed lines). The shaded areas denote the 95% confidence intervals of Monte Carlo experiments. However, for RCC, the 95% confidence intervals are very small.

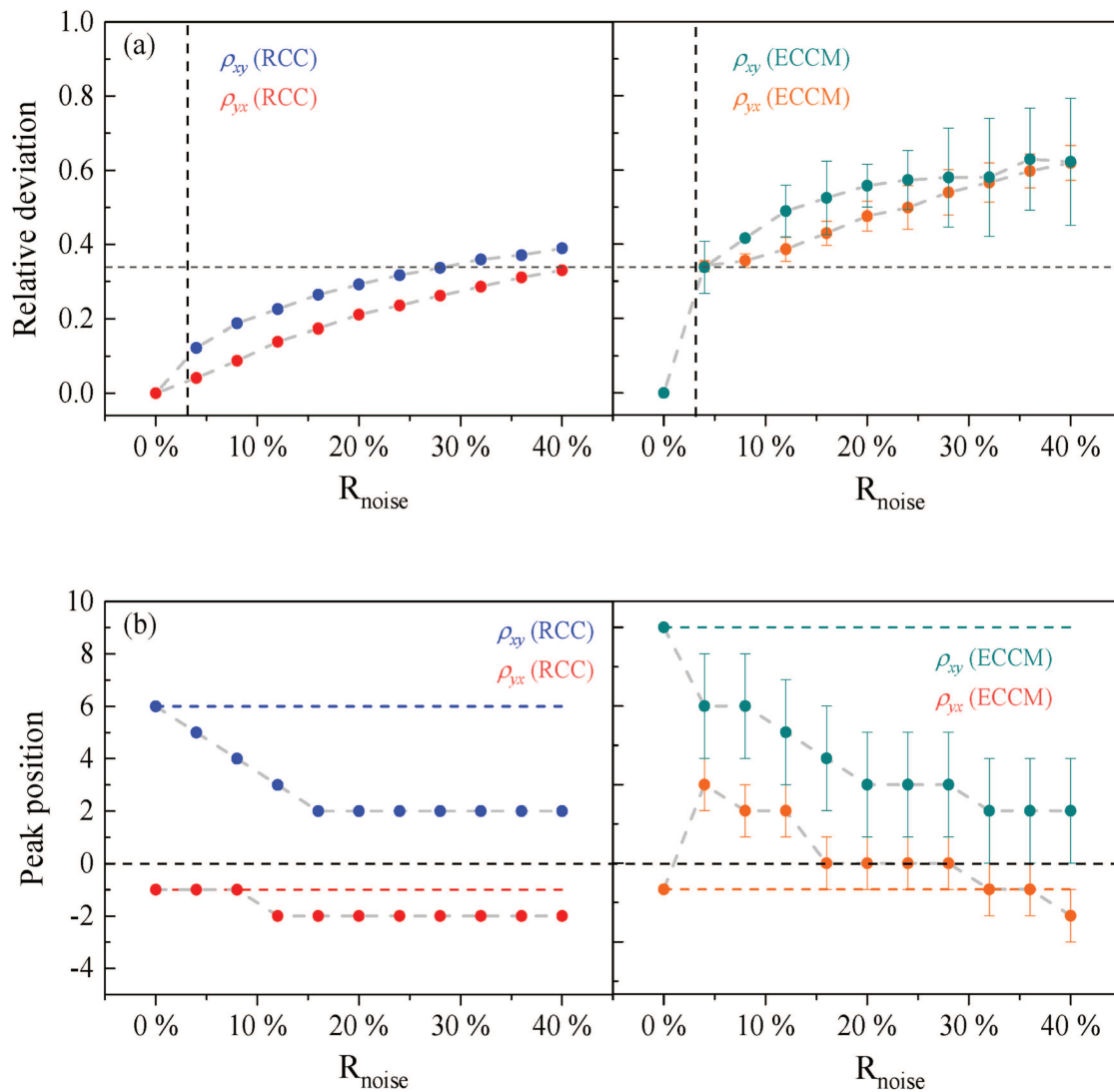


**FIG. 6.** (a) Relative deviation of the prediction skill induced by noise. (b) Varying peak position induced by noise. Left is for RCC and right for ECCM. The colored dashed lines are for the peak positions in cases without noise. The error bars denote the 95% confidence intervals from Monte Carlo experiments (for each Monte Carlo simulation, we generated a new Gaussian-distributed white noise sequence for adding to the time series before computing RCC). However, for RCC, the 95% confidence intervals are very small, so that the error bars are not distinguishable in (a) and (b).

## VI. APPLICATION TO COMPLEX SYSTEMS

Our comparison between RCC and ECCM has demonstrated the ability of RCC to infer causal relationships, including causal direction and coupling delay. There are many interacting variables in a real-world complex system, and identifying their causal relationships is useful to understand the dynamics of complex system.<sup>14</sup> In the following, we will present two applications of RCC to complex systems.

**TABLE I.** Given time series with length of 10 000 and the same computer (the CPU speed: 3.6 GHz), estimation for time consumption of using RCC and ECCM. The computational time includes the sum of training and testing periods for both RCC and ECCM. Here, phase space parameters (embedding dimensionality and delay time) are calculated by means of the false nearest neighbor algorithm.<sup>2–7</sup>

	RCC	ECCM (phase space parameters)
Computational time	≈90 s	≈1500 s (≈1200 s)

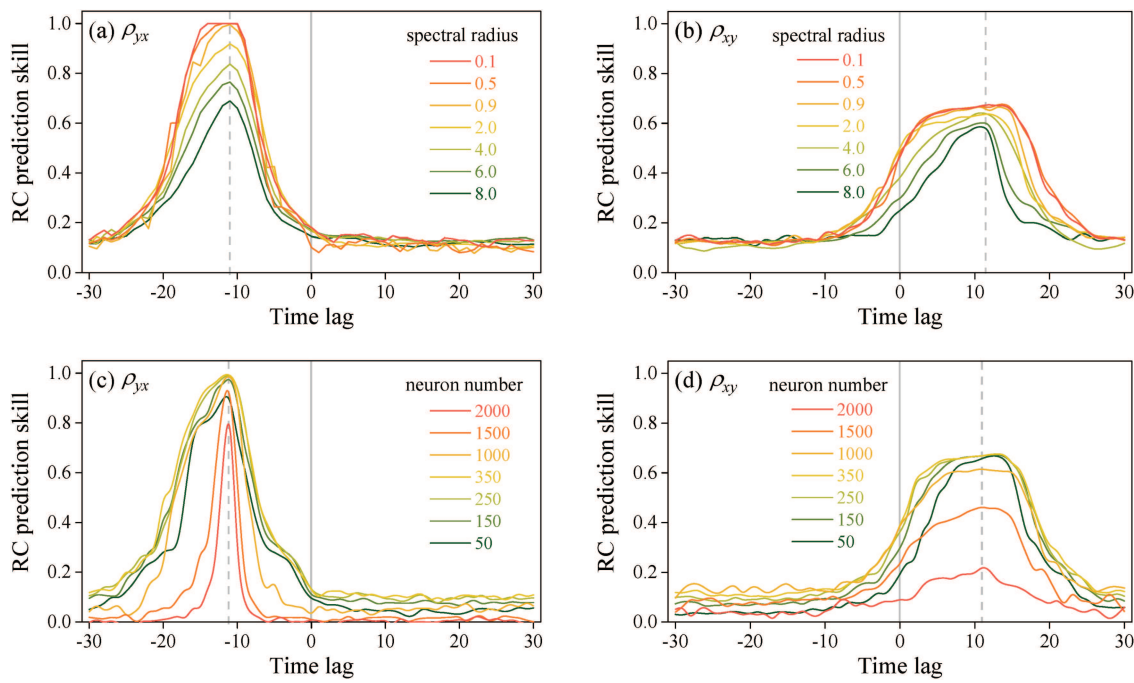


**FIG. 7.** Experimenting the reservoir parameters with different values, the results of RCC applied to the system of Eq. (11) ( $\tau_d = 10$ ). Horizontal axis denotes the used time lag for the RC prediction. Setting spectral radius to different values (neuron number is fixed to 400), the different RCC curves are shown: (a) for using  $y(t)$  to predict  $x(t + \tau)$ , and (b) for using  $x(t)$  to predict  $y(t + \tau)$ . Setting the number of reservoir neurons to different values (spectral radius is fixed to 1.0), the different RCC curves are shown: (c) for using  $y(t)$  to predict  $x(t + \tau)$ , and (d) for using  $x(t)$  to predict  $y(t + \tau)$ .

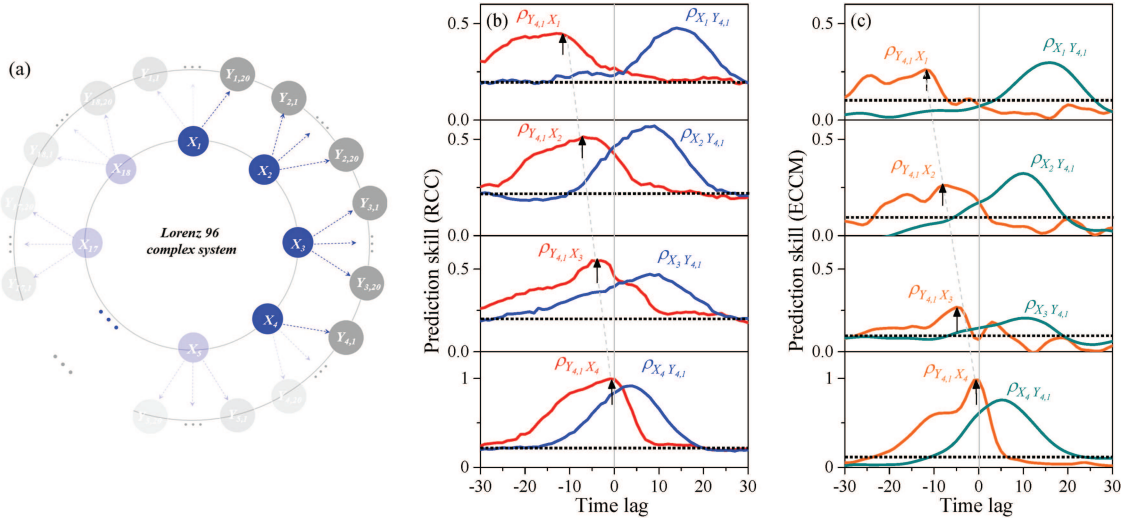


**FIG. 8.** (a) Diagram of a variant of the two-level Lorenz 96 system [Eq. (13)] with some remote interacting variables indicated. (b) RCC: Using  $Y_{4,1}$  to predict  $X_1, X_2, X_3$ , and  $X_4$  (red line), and using  $X_1, X_2, X_3$ , and  $X_4$  to predict  $Y_{4,1}$  (blue line). (c) ECCM: Using  $Y_{4,1}$  to predict  $X_1, X_2, X_3$ , and  $X_4$  (orange line), and using  $X_1, X_2, X_3$ , and  $X_4$  to predict  $Y_{4,1}$  (green line). The horizontal dotted lines represent the upper 95% confidence level of the IAAFT surrogate test.

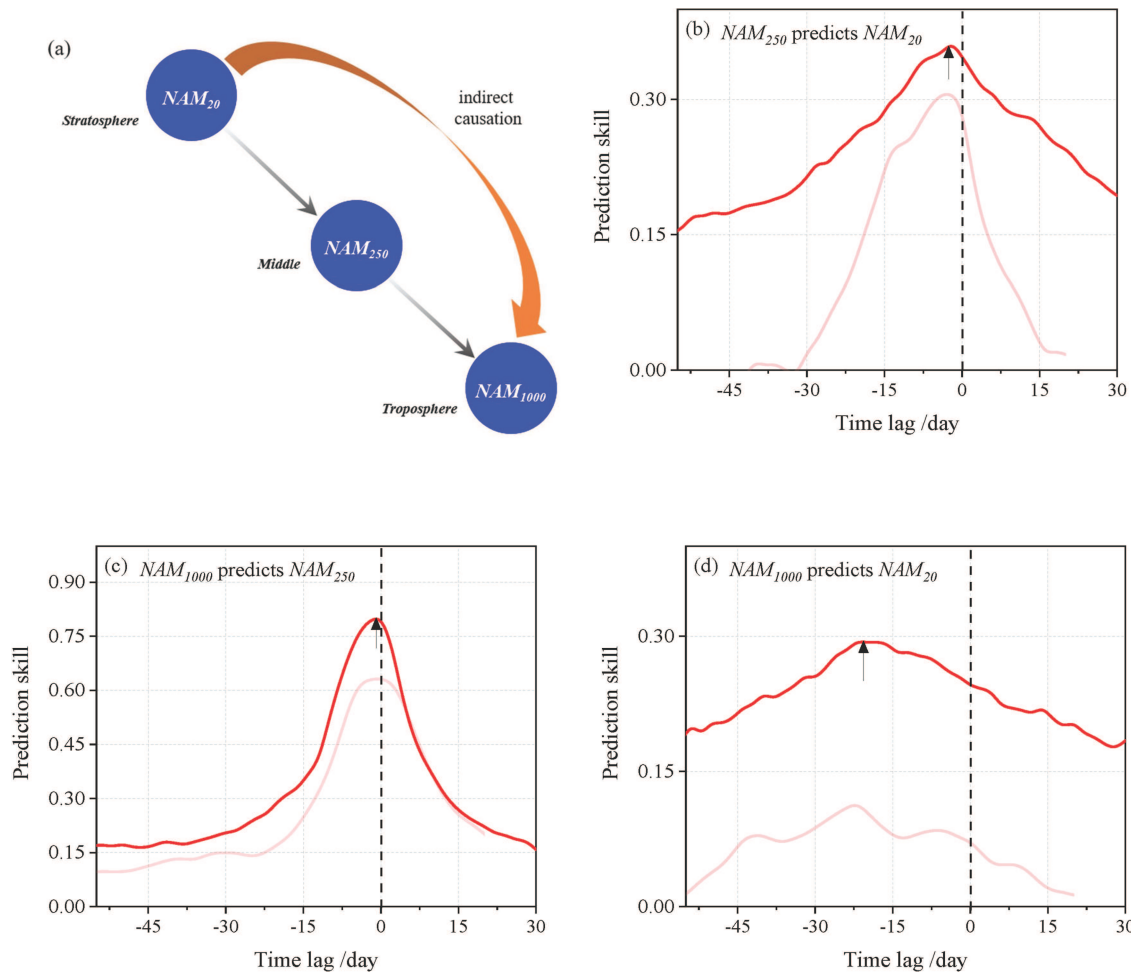


**FIG. 9.** (a) Causal chain relation in the stratosphere–troposphere coupling:  $NAM_{20}$  causes  $NAM_{250}$  and  $NAM_{250}$  causes  $NAM_{1000}$ , such that  $NAM_{20}$  indirectly causes  $NAM_{1000}$ . (b) Prediction skill by using  $NAM_{250}$  to predict  $NAM_{20}$ , the optimal skill occurs at lag = -2. (c) Prediction skill by using  $NAM_{1000}$  to predict  $NAM_{250}$ , the optimal skill occurs at lag = -1. (d) Prediction skill by using  $NAM_{1000}$  to predict  $NAM_{20}$ , the optimal skill occurs at lag = -21. Darker and lighter lines are the results of RCC and ECCM methods, respectively. All maxima of the curves have exceeded the upper 95% confidence level of IAAFT surrogate test.

### A. Remote causal interactions in a high-dimensional dynamical system

In complex systems, there often exist variables that are connected through remote indirect interactions<sup>10,14,19</sup> (such as teleconnections in the climate system<sup>47,48</sup>), and identifying the transitive causal chain or teleconnection path in such a background is useful.<sup>14,48</sup> Here, we check whether RCC and ECCM can be used to identify the causal chain in high-dimensional dynamics. The high-dimensional Lorenz 96 chaotic system is commonly used to mimic the atmospheric system,<sup>49,50</sup> and the conclusions from this system often have implications for solving real-world problems. We use a

variant of the Lorenz 96 system given by<sup>49</sup>

$$\begin{aligned} \frac{dX_i}{dt} &= X_{i-1}(X_{i+1} - X_{i-2}) - X_i + F, \\ \frac{dY_{ij}}{dt} &= \theta[Y_{ij+1}(Y_{ij-1} - Y_{ij+2}) - Y_{ij} + X_i]. \end{aligned} \quad (13)$$

where  $X_i$  ( $i = 1, \dots, 18$ ) and  $Y_{ij}$  ( $j = 1, \dots, 20$ ) denote the model variables, and  $F$  is the external forcing ( $F = 10$ ). Each  $X_i$  is connected to  $Y_{ij}$  with a unidirectional coupling. Meanwhile, the parameter  $\theta$  controls the coupling strength between the two levels (we set  $\theta$  to 10). We use a fourth order Runge–Kutta method, a time step size of 0.05,

and periodic boundary conditions (that is  $X_0 = X_I$  and  $X_{I+1} = X_1$ ;  $Y_{i,0} = Y_{i-1,I}$  and  $Y_{i,I+1} = Y_{i+1,1}$ ). Figure 8(a) illustrates how the variables are connected in this system.

As Fig. 8(a) shows, the connection between  $X_1$  and  $Y_{4,1}$  is through a transitive route and the shortest path is “ $X_1 \rightarrow X_2 \rightarrow X_3 \rightarrow X_4 \rightarrow Y_{4,1}$ .” For the RCC result, the maxima of  $\rho_{Y_{4,1}X_1}$ ,  $\rho_{Y_{4,1}X_2}$ ,  $\rho_{Y_{4,1}X_3}$ , and  $\rho_{Y_{4,1}X_4}$  occur at lags of  $-12$ ,  $-7$ ,  $-4$ , and  $-1$  [Fig. 8(b)], respectively. Since the maximum lag occurs at a negative lag, this indicates the coupling delay between the two corresponding variables. The occurrence order of these lags means that, among the four variables,  $X_1$  is the earliest one influencing  $Y_{4,1}$ , and  $X_4$  is the latest. The inferred order of this causal chain by RCC is consistent with the real structure of this transitive causal chain. For  $\rho_{X_1Y_{4,1}}$ ,  $\rho_{X_2Y_{4,1}}$ ,  $\rho_{X_3Y_{4,1}}$ , and  $\rho_{X_4Y_{4,1}}$ , their maxima occur at different positive lags, and the occurrence order of these maximum lags is also influenced by the order of the causal chain. We also tested these time series output from Eq. (13) when the integration step size was  $0.01$ ,  $0.05$ , and  $0.1$  respectively, and the inferred results of causal chain by RCC are consistent to one another (not shown).

Figure 8(c) shows the results of ECCM applied to the same high-dimensional system, where we use  $m = 3$  and  $\tau_0 = 1$  as the phase space parameters of ECCM. The maxima of  $\rho_{Y_{4,1}X_1}$ ,  $\rho_{Y_{4,1}X_2}$ ,  $\rho_{Y_{4,1}X_3}$ , and  $\rho_{Y_{4,1}X_4}$  occur at lags of  $-12$ ,  $-7$ ,  $-4$ , and  $-1$ , respectively, which is identical to the results of RCC, whereas the peak values of  $\rho_{Y_{4,1}X_1}$ ,  $\rho_{Y_{4,1}X_2}$ ,  $\rho_{Y_{4,1}X_3}$ , and  $\rho_{Y_{4,1}X_4}$  are all smaller than that of RCC. Specifically, there are multiple peaks in the curve of  $\rho_{Y_{4,1}X_3}$  [see the third panel in Figs. 8(c)]: the first peak that occurs at lag  $= -4$  is consistent with the result of RCC, but for the second peak occurring at lag  $= 3$ , it is difficult to explain the occurrence of this peak (although it is not the maximum). Similarly, there also exist multiple peaks for other ECCM curves [Fig. 8(c)]. However, for the results of RCC applied to this high-dimensional system [Fig. 8(b)], there is no presence of such multiple peaks and, thus, the inference for causal direction and coupling delay with RCC is more robust.

## B. Stratosphere-troposphere coupling

The Northern Annular Mode (NAM) is a large-scale atmospheric pattern that has a significant impact on surface weather and climate conditions over Europe, Russia, and the United States on subseasonal to decadal time scales,<sup>6,51–57</sup> and the NAM index time series at different vertical levels can respectively represent the temporal variability of atmosphere subsystems at different heights.<sup>51–53</sup> We compute the NAM index time series using daily geopotential height over the region  $20^\circ\text{N}$ – $90^\circ\text{N}$  and  $-180^\circ\text{E}$ – $180^\circ\text{E}$  for the period of 1979 through 2018 (provided by the National Center for Atmospheric Research/National Center for Environmental Prediction reanalysis<sup>58,59</sup>). The annual cycle was removed from the data by subtracting the long-term climatological average for each calendar day of each year. Then, empirical orthogonal decomposition was applied to the data at each pressure level, where the first component of the decomposition denotes the NAM at each pressure level.<sup>51–56</sup>

We select the NAM index time series at the levels of  $20\text{ hPa}$ ,  $250\text{ hPa}$ , and  $1000\text{ hPa}$ , and call them  $NAM_{20}$ ,  $NAM_{250}$ , and  $NAM_{1000}$ , respectively. As Fig. 9(a) shows,  $1000\text{ hPa}$  and  $20\text{ hPa}$  correspond to the lower troposphere and the upper stratosphere,

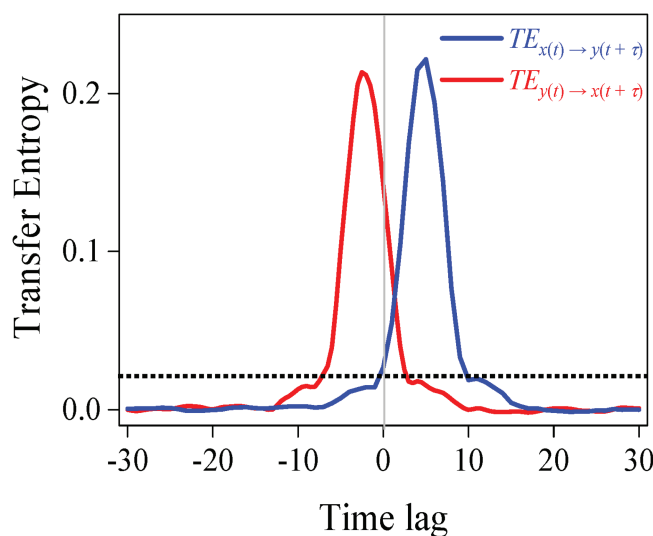
respectively, and  $250\text{ hPa}$  represents the upper troposphere. Previous studies<sup>52–54</sup> revealed that the activity of the Northern Hemispheric polar vortex will induce a propagation of energy from the stratosphere to the troposphere, and the information about these causal interactions is encoded in these NAM index time series. However, previous studies also reported that linear regression methods cannot extract the information about these interactions,<sup>19</sup> due to the nonlinearity of the NAM index time series.<sup>55–57</sup> Now, applying RCC and ECCM to the NAM index, we confirm the power of RCC in detecting the causal chain in a real-world dataset.

Figure 9(b) shows the time-lagged prediction skill for using  $NAM_{250}$  to predict  $NAM_{20}$  by RCC, where the optimal skill occurs at lag  $= -2$  days. Then, in Fig. 9(c), the optimal skill occurs at lag  $= -1$  for using  $NAM_{1000}$  to predict  $NAM_{250}$  by RCC. It means that  $NAM_{20}$  causes  $NAM_{250}$ , and  $NAM_{250}$  causes  $NAM_{1000}$ . Will  $NAM_{20}$  (at the stratosphere) further cause  $NAM_{1000}$  (at the troposphere)? Figure 9(d) shows that the optimal skill occurs at lag  $= -23$  days for using  $NAM_{1000}$  to predict  $NAM_{20}$  by RCC. This reveals that  $NAM_{20}$  indeed causes  $NAM_{1000}$ . For the results of ECCM, the peak positions are identical to that of RCC where we use  $m = 5$  and  $\tau_0 = 1$  as the phase space parameters of ECCM. Previous work<sup>52–54</sup> employed numerical climate models and composite analysis to investigate polar vortex energy propagating from stratosphere to troposphere, whose propagation time was around three weeks. Our results with RCC and ECCM are consistent with these results.

## VII. CONCLUSIONS AND DISCUSSION

Here we compared existing causality identification methods with a neural network based causal method. The phase space prediction based ECCM method<sup>10,19</sup> is able to detect causal relationships from time series, including the causal direction, causality intensity, and coupling delay. However, considering some shortcomings of ECCM, we developed the reservoir computing based method RCC to address the issues. Similar to some existing causality methods,<sup>10,12,13</sup> such as Granger method and ECCM, RCC uses a prediction model to detect causality, but it has superior efficiency and robustness. Our study demonstrates that the main advantages of RCC over ECCM are as follows: (i) better robustness to noise and (ii) improved computational efficiency. RCC is skillful for detecting the true causality direction and coupling delay in real-world data.

We also carried out a comparison with transfer entropy<sup>7,8,13,60</sup> to further inspect the causal detection mechanism of RCC. When considering time-lagged statistics for transfer entropy<sup>11,61,62</sup> of two variables, it can be detected whether there exists information carried forward through time between the two variables. Figure 10 shows the results of transfer entropy applied to the system of Eq. (9) ( $C = 0.8$ ), where the time-lagged statistic is considered.  $TE_{x(t) \rightarrow y(t+\tau)}$  denotes the transferred information from  $x(t)$  to  $y(t+\tau)$  that is measured by transfer entropy: its maximum occurs at a positive lag, and for other time lags,  $TE_{x(t) \rightarrow y(t+\tau)}$  gets smaller and is not even statistically significant.  $TE_{y(t) \rightarrow x(t+\tau)}$  denotes the measured transfer information from  $y(t)$  to  $x(t+\tau)$ , and its maximum occurs at a negative lag. This means that the information of  $x$  is transferred to  $y$  forward through time (the current information content of  $y$  is partially transferred from the contents of  $x$  at previous time points). This result is consistent with that of RCC and ECCM [Fig. 3(a)],



**FIG. 10.** The results of transfer entropy measurement applied to the system of Eq. (9) ( $C = 0.8$ ).  $TE_{x(t) \rightarrow y(t+\tau)}$  denotes the transferred information from  $x(t)$  to  $y(t+\tau)$  (blue line) measured by transfer entropy, and  $TE_{y(t) \rightarrow x(t+\tau)}$  denotes the transferred information from  $y(t)$  to  $x(t+\tau)$  (red line) measured by transfer entropy. The horizontal dotted line represents the upper 95% confidence level of IAAFT surrogate test.

and the transferred information forward through time is the origin of predictability with the reservoir computer and phase space prediction models.<sup>8,10,11,13,15,24</sup> Moreover, here the computational time of the transfer entropy with time-lagged statistics is 2100 s, which is much longer than that of ECCM (1500 s) and of RCC (90 s) in the same case (see Table I).

Moreover, how the network state of RC is responding to these causal relationships is an open question due to the “black box” nature of neural networks. A better understanding of how the neural network organizes itself, and the mechanisms in which reservoir network parameters<sup>31–38</sup> determine its prediction skill, is needed to increase the reliability and generalizability of our approach.

## ACKNOWLEDGMENTS

We acknowledge the websites (<https://cran.r-project.org/src/contrib/Archive/rEDM/>) for providing the instructional algorithm for ECCM. We also acknowledge the National Center for Environmental Prediction reanalysis (<https://www.esrl.noaa.gov/psd/data/gridded/data.ncep.reanalysis2.html>) for providing the atmospheric dataset.

We thank the anonymous reviewers for their constructive comments and suggestions. We acknowledge the thoughtful suggestions of Dr. Lin Piao for this paper. Y.H. and Z.F. acknowledge the support from the National Natural Science Foundation of China through Grant Nos. 41675049 and 41475048. C.F. was supported by the Collaborative Research Centre TRR 181 “Energy Transfer

in Atmosphere and Ocean,” funded by the Deutsche Forschungsgemeinschaft (DFG, German Research Foundation) (Project No. 274762653).

## DATA AVAILABILITY

All codes and data involved in this paper are available on request from the authors.

## REFERENCES

- 1 C. W. Granger, “Investigating causal relations by econometric models and cross-spectral methods,” *Econometrica* **37**, 424–438 (1969).
- 2 G. Sugihara, R. May, H. Ye, C. H. Hsieh, E. Deyle, M. Fogarty, and S. Munch, “Detecting causality in complex ecosystems,” *Science* **338**(6106), 496–500 (2012).
- 3 M. Palus, V. Komarek, T. Prochazka, Z. Hrcnir, and K. Sterbova, “Synchronization and information flow in EEGs of epileptic patients,” *IEEE Eng. Med. Biol. Mag.* **20**(5), 65–71 (2001).
- 4 S. Vannitsem and P. Ekelmans, “Causal dependences between the coupled ocean–atmosphere dynamics over the tropical pacific, the North Pacific and the North Atlantic,” *Earth Syst. Dyn.* **9**(3), 1063–1083 (2018).
- 5 S. Vannitsem, Q. Dalaïden, and H. Goosse, “Testing for dynamical dependence: Application to the surface mass balance over Antarctica,” *Geophys. Res. Lett.* **46**(21), 12125–12135 (2019).
- 6 N. N. Zhang, G. L. Wang, and A. A. Tsonis, “Dynamical evidence for causality between Northern Hemisphere annular mode and winter surface air temperature over Northeast Asia,” *Clim. Dyn.* **52**, 3175–3182 (2019).
- 7 T. Schreiber, “Measuring information transfer,” *Phys. Rev. Lett.* **85**(2), 461 (2000).
- 8 K. Hlaváčková-Schindler, M. Paluš, M. Vejmelka, and J. Bhattacharya, “Causality detection based on information-theoretic approaches in time series analysis,” *Phys. Rep.* **441**(1), 1–46 (2007).
- 9 A. Montalto, S. Stramaglia, L. Faes, G. Tessitore, R. Prevete, and D. Marinazzo, “Neural networks with non-uniform embedding and explicit validation phase to assess Granger causality,” *Neural Networks* **71**, 159–171 (2015).
- 10 H. Ye, E. R. Deyle, L. J. Gilarranz, and G. Sugihara, “Distinguishing time-delayed causal interactions using convergent cross mapping,” *Sci. Rep.* **5**, 14750 (2015).
- 11 D. Coufal, J. Jakubík, N. Jajcay, J. Hlinka, A. Krakovská, and M. Paluš, “Detection of coupling delay: A problem not yet solved,” *Chaos* **27**(8), 083109 (2017).
- 12 A. Krakovská, J. Jakubík, M. Chvosteková, D. Coufal, N. Jajcay, and M. Paluš, “Comparison of six methods for the detection of causality in a bivariate time series,” *Phys. Rev. E* **97**(4), 042207 (2018).
- 13 M. Paluš, A. Krakovská, J. Jakubík, and M. Chvosteková, “Causality, dynamical systems and the arrow of time,” *Chaos* **28**(7), 075307 (2018).
- 14 J. Runge, S. Bathiany, E. Boltt, G. Camps-Valls, D. Coumou, E. Deyle, C. Glymour, M. Kretschmer, M. D. Mahecha, J. Muñoz-Marí, E. H. Van Nes, J. Peter, R. Quax, M. Reichstein, M. Scheffer, B. Schölkopf, P. Spirtes, G. Sugihara, J. Sun, K. Zhang, and J. Zscheischler, “Inferring causation from time series in earth system sciences,” *Nat. Commun.* **10**(1), 2553 (2019).
- 15 F. Takens, “Detecting strange attractors in turbulence,” in *Dynamical Systems and Turbulence, Lecture Notes in Mathematics* (Springer, 1981), Vol. 898, pp. 366–381.
- 16 Y. Malevergne and D. Sornette, *Extreme Financial Risks From Dependence to Risk Management* (Springer Science & Business Media, 2006).
- 17 E. R. Deyle and G. Sugihara, “Generalized theorems for nonlinear state space reconstruction,” *PLoS One* **6**(3), e18295 (2011).
- 18 J. M. McCracken and R. S. Weigel, “Convergent cross-mapping and pairwise asymmetric inference,” *Phys. Rev. E* **90**(6), 062903 (2014).
- 19 Y. Huang, C. L. Franzke, N. Yuan, and Z. Fu, “Systematic identification of causal relations in high-dimensional chaotic systems application to stratosphere-troposphere coupling,” *Clim. Dyn.* (submitted) (2019).
- 20 N. F. Rulkov, M. M. Sushchik, L. S. Tsimring, and H. D. I. Abarbanel, “Generalized synchronization of chaos in directionally coupled chaotic systems,” *Phys. Rev. E* **51**, 980–994 (1995).

- <sup>21</sup>A. A. Tsonis, E. R. Deyle, H. Ye, and G. Sugihara, "Convergent cross mapping: Theory and an example," in *Advances in Nonlinear Geosciences* (Springer, Cham, 2018), pp. 587–600.
- <sup>22</sup>N. Jaćay, S. Kravtsov, G. Sugihara, A. A. Tsonis, and M. Paluš, "Synchronization and causality across time scales in El Niño Southern Oscillation," *NPJ Clim. Atmos. Sci.* **1**(1), 33 (2018).
- <sup>23</sup>T. Buzug and G. Pfister, "Comparison of algorithms calculating optimal embedding parameters for delay time coordinates," *Physica D* **58**(1–4), 127–137 (1992).
- <sup>24</sup>M. Casdagli, S. Eubank, J. D. Farmer, and J. Gibson, "State space reconstruction in the presence of noise," *Physica D* **51**(1–3), 52–98 (1991).
- <sup>25</sup>D. Kugiumtzis, "State space reconstruction parameters in the analysis of chaotic time series—The role of the time window length," *Physica D* **95**(1), 13–28 (1996).
- <sup>26</sup>A. Casaleggio and S. Braiotta, "Estimation of Lyapunov exponents of ECG time series—The influence of parameters," *Chaos Solitons Fractals* **8**(10), 1591–1599 (1997).
- <sup>27</sup>R. Hegger and H. Kantz, "Improved false nearest neighbor method to detect determinism in time series data," *Phys. Rev. E* **60**(4), 4970 (1999).
- <sup>28</sup>A. Sitz, U. Schwarz, J. Kurths, and H. U. Voss, "Estimation of parameters and unobserved components for nonlinear systems from noisy time series," *Phys. Rev. E* **66**(1), 016210 (2002).
- <sup>29</sup>A. A. Tsonis, "Reconstructing dynamics from observables: The issue of the delay parameter revisited," *Int. J. Bifurcation Chaos* **17**(12), 4229–4243 (2007).
- <sup>30</sup>D. Mönster, R. Fusaroli, K. Tylén, A. Roepstorff, and J. F. Sherson, "Causal inference from noisy time-series data—Testing the convergent cross-mapping algorithm in the presence of noise and external influence," *Future Gener. Comput. Syst.* **73**, 52–62 (2017).
- <sup>31</sup>M. Lukoševičius and H. Jaeger, "Reservoir computing approaches to recurrent neural network training," *Comput. Sci. Rev.* **3**(3), 127–149 (2009).
- <sup>32</sup>J. Pathak, Z. Lu, B. R. Hunt, M. Girvan, and E. Ott, "Using machine learning to replicate chaotic attractors and calculate Lyapunov exponents from data," *Chaos* **27**(12), 121102 (2017).
- <sup>33</sup>C. Du, F. Cai, M. A. Zidan, W. Ma, S. H. Lee, and W. D. Lu, "Reservoir computing using dynamic memristors for temporal information processing," *Nat. Commun.* **8**(1), 2204 (2017).
- <sup>34</sup>Z. Lu, J. Pathak, B. Hunt, M. Girvan, R. Brockett, and E. Ott, "Reservoir observers: Model-free inference of unmeasured variables in chaotic systems," *Chaos* **27**(4), 041102 (2017).
- <sup>35</sup>Z. Lu, B. R. Hunt, and E. Ott, "Attractor reconstruction by machine learning," *Chaos* **28**(6), 061104 (2018).
- <sup>36</sup>J. Pathak, B. Hunt, M. Girvan, Z. Lu, and E. Ott, "Model-free prediction of large spatiotemporally chaotic systems from data: A reservoir computing approach," *Phys. Rev. Lett.* **120**(2), 024102 (2018).
- <sup>37</sup>A. Chattopadhyay, P. Hassanzadeh, K. Palem, and D. Subramanian, "Data-driven prediction of a multi-scale Lorenz 96 chaotic system using a hierarchy of deep learning methods reservoir computing, ANN, and RNN-LSTM," *arXiv:1906.08829* (2019).
- <sup>38</sup>Y. Huang, L. Yang, and Z. Fu, "Reconstructing coupled time series in climate systems by machine learning," *Earth Syst. Dyn. Discuss.* (submitted) (2019).
- <sup>39</sup>M. Reichstein, G. Camps-Valls, B. Stevens, M. Jung, J. Denzler, and N. Carvalhais, "Deep learning and process understanding for data-driven earth system science," *Nature* **566**(7743), 195 (2019).
- <sup>40</sup>P. Erdős and A. Rényi, "On random graphs," *Publicationes Mathematicae* **6**(26), 290–297 (1959).
- <sup>41</sup>T. Schreiber and A. Schmitz, "Improved surrogate data for nonlinearity tests," *Phys. Rev. Lett.* **77**(4), 635 (1996).
- <sup>42</sup>J. H. Lucio, R. Valdés, and L. R. Rodríguez, "Improvements to surrogate data methods for nonstationary time series," *Phys. Rev. E* **85**(5), 056202 (2012).
- <sup>43</sup>N. Marwan, J. F. Donges, Y. Zou, R. V. Donner, and J. Kurths, "Complex network approach for recurrence analysis of time series," *Phys. Lett. A* **373**(46), 4246–4254 (2009).
- <sup>44</sup>Z. Lu, N. Yuan, and Z. Fu, "Percolation phase transition of surface air temperature networks under attacks of El Niño/La Niña," *Sci. Rep.* **6**, 26779 (2016).
- <sup>45</sup>T. Weng, J. Zhang, M. Small, R. Zheng, and P. Hui, "Memory and betweenness preference in temporal networks induced from time series," *Sci. Rep.* **7**, 41951 (2017).
- <sup>46</sup>Y. Huang, Q. Deng, and Z. Fu, "Could network analysis of horizontal visibility graphs be faithfully used to infer long-term memory properties in real-world time series?," *Commun. Nonlinear Sci.* **79**, 104908 (2019).
- <sup>47</sup>S. B. Feldstein and C. L. Franzke, "Atmospheric teleconnection patterns," in *Nonlinear and Stochastic Climate Dynamics* (Cambridge University Press, 2017), pp. 54–104.
- <sup>48</sup>D. Zhou, A. Gozolchiani, Y. Ashkenazy, and S. Havlin, "Teleconnection paths via climate network direct link detection," *Phys. Rev. Lett.* **115**(26), 268501 (2015).
- <sup>49</sup>E. N. Lorenz, "Predictability: A problem partly solved," in *ECMWF Seminar on Predictability, Reading, United Kingdom, 4–8 September 1995* (ECMWF, 1996), Vol. I, pp. 40–58.
- <sup>50</sup>D. S. Wilks, "Effects of stochastic parametrizations in the Lorenz'96 system," *Q. J. Roy. Meteorol. Soc.* **131**(606), 389–407 (2005).
- <sup>51</sup>D. W. Thompson and J. M. Wallace, "Regional climate impacts of the Northern Hemisphere annular mode," *Science* **293**(5527), 85–89 (2001).
- <sup>52</sup>M. P. Baldwin, D. B. Stephenson, D. W. Thompson, T. J. Dunkerton, A. J. Charlton, and A. O'Neill, "Stratospheric memory and skill of extended-range weather forecasts," *Science* **301**(5633), 636–640 (2003).
- <sup>53</sup>M. P. Baldwin and D. W. Thompson, "A critical comparison of stratosphere-troposphere coupling indices," *Q. J. Roy. Meteorol. Soc.* **135**(644), 1661–1672 (2009).
- <sup>54</sup>E. P. Gerber and L. M. Polvani, "Stratosphere-troposphere coupling in a relatively simple AGCM: The importance of stratospheric variability," *J. Clim.* **22**(8), 1920–1933 (2009).
- <sup>55</sup>S. M. Osprey and M. H. Ambaum, "Evidence for the chaotic origin of northern annular mode variability," *Geophys. Res. Lett.* **38**(15), L15702 (2011).
- <sup>56</sup>Z. Fu, L. Shi, F. Xie, and L. Piao, "Nonlinear features of northern annular mode variability," *Physica A* **449**, 390–394 (2016).
- <sup>57</sup>D. Nian and Z. Fu, "Contrasting stratospheric-tropospheric multifractal behaviors in NAM variability," *Clim. Dyn.* **54**, 37–52 (2019).
- <sup>58</sup>E. Kalnay, M. Kanamitsu, R. Kistler, W. Collins, D. Deaven, L. Gandin, and Y. Zhu, "The NCEP/NCAR 40-year reanalysis project," *Bull. Am. Meteorol. Soc.* **77**(3), 437–472 (1996).
- <sup>59</sup>M. Kanamitsu, W. Ebisuzaki, J. Woollen, S. K. Yang, J. J. Hnilo, M. Fiorino, and G. L. Potter, "NCEP-DOE AMIP-II reanalysis (R-2)," *Bull. Am. Meteorol. Soc.* **83**(11), 1631–1644 (2002).
- <sup>60</sup>M. Paluš, V. Komárek, Z. Hrnčíř, and K. Štěrbová, "Synchronization as adjustment of information rates: Detection from bivariate time series," *Phys. Rev. E* **63**(4), 046211 (2001).
- <sup>61</sup>M. Vejmelka and M. Paluš, "Inferring the directionality of coupling with conditional mutual information," *Phys. Rev. E* **77**(2), 026214 (2008).
- <sup>62</sup>J. Runge, J. Heitzig, V. Petoukhov, and J. Kurths, "Escaping the curse of dimensionality in estimating multivariate transfer entropy," *Phys. Rev. Lett.* **108**(25), 258701 (2012).